Published in final edited form as:
Nat Cell Biol. ; 13(10): 1214–1223. doi:10.1038/ncb2332.

Midbody accumulation through evasion of autophagy contributes to cellular reprogramming and tumorigenicity

Tse-Chun Kuo[1,9], **Chun-Ting Chen**[1,9], **Desiree Baron**[1], **Tamer T. Onder**[2,3,4,5], **Sabine Loewer**[2,3,4,5], **Sandra Almeida**[6], **Cara Weismann**[1,6], **Ping Xu**[1], **Jean-Marie Houghton**[7], **Fen-Biao Gao**[6], **George Q. Daley**[2,3,4,5,8], and **Stephen Doxsey**[1,10]

[1]Program in Molecular Medicine, University of Massachusetts Medical School, Worcester, Massachusetts 01605, USA

[2]Stem Cell Program, Children's Hospital Boston, Boston, Massachusetts 02115, USA

[3]Stem Cell Transplantation Program, Division of Pediatric Hematology and Oncology, Manton Center for Orphan Disease Research, Children's Hospital Boston and Dana Farber Cancer Institute, Boston, Massachusetts 02115, USA

[4]Department of Biological Chemistry and Molecular Pharmacology, Harvard Medical School, Boston, Massachusetts 02115, USA

[5]Harvard Stem Cell Institute, Cambridge, Massachusetts 02138, USA

[6]Departments of Neurology, University of Massachusetts Medical School, Worcester, Massachusetts 01605, USA

[7]Department of Pathology, University of Massachusetts Medical School, Worcester, Massachusetts 01605, USA

[8]Howard Hughes Medical Institute, Chevy Chase, Maryland 20815, USA

Abstract

The midbody (MB) is a singular organelle formed between daughter cells during cytokinesis and required for their final separation. MBs persist in cells long after division as midbody derivatives (MB^ds), but their fate is unclear. Here we show that MB^ds are inherited asymmetrically by the daughter cell with the older centrosome. They selectively accumulate in stem cells, induced pluripotent stem cells (iPSCs) and potential cancer 'stem cells' (CSCs) *in vivo* and *in vitro*. MB^d loss accompanies stem cell differentiation, and involves autophagic degradation mediated by binding of the autophagic receptor, NBR1, to the MB protein Cep55. Differentiating cells and

[10]Correspondence should be addressed to S.J.D. (stephen.doxsey@umassmed.edu).
[9]These authors contributed equally to this work

AUTHOR CONTRIBUTIONS

C-T.C. and S.J.D. conceived the project and wrote the manuscript with the help of T-C.K. and D.M.B. The experiments on the inheritance and localization of MB^ds as well as some for MB^d degradation were conducted by C-T.C. The experiments on MB^d accumulation were conducted by C-T.C. with the help of T-C.K. and C.M.W. Investigation of the mechanisms for MB^d degradation was conceived by T-C.K. and S.J.D., and much of the work executed by T-C.K. Autophagic flux assay, soft-agar assay of FACS-isolated cells, and MB^d localization in neural progenitors were conducted by D.M.B., who contributed substantially to the work and intellectual input on multiple aspects of this project. The reprogramming assay was conducted and analyzed by T-C.K., T.T.O, and S.L. The preparation of hESCs for live-imaging was conducted by S.A. Tissue preparation was assisted by P.X. and J.M.H.

normal dividing cells do not accumulate MB^{d}s and possess high autophagic activity. Stem cells and cancer cells accumulate MB^{d}s by evading autophagosome encapsulation and exhibit low autophagic activity. MB^{d} enrichment enhances reprogramming to iPSCs and increases *in vitro* tumorigenicity of cancer cells. These results suggest unexpected roles for MB^{d}s in stem cells and CSCs.

INTRODUCTION

Cell division culminates in the separation of two genetically identical daughter cells[1]. During division, cell fate determinants segregate asymmetrically to stem cell progeny[2]. The two spindle poles organized by differentially-aged centrosomes contribute to this asymmetry[2,3] in that the older centrosome is inherited by the daughter cell that retains the stem cell fate[4-6].

Abscission completes cell division by severing the intercellular bridge between the two future daughter cells[1,7]. Within the intercellular bridge lies the midbody (MB), a large proteinaceous organelle[7-10] that was previously thought to detach from cells and disintegrate extracellularly as a remnant[7,8]. Recent studies show that post-abscission MBs or MB derivatives (MB^{d}s) can be retained by daughter cells, suggesting alternative fates for these organelles[9,11,12].

The fate and function of MB^{d}s is unclear. In neural progenitors, MB^{d}s possess the putative stem cell marker CD133/prominin-1 and are proposed to participate in intercellular signaling during neural development[13,14]. MB^{d}s can be degraded by autophagy (see below)[12], but the relationship between MB^{d} loss or retention and the physiological state of cells is unknown.

During autophagy (macroautophagy), double membrane-bound autophagosomes assemble, engulf cytoplasmic material, and fuse with lysosomes for degradation[15-18]. Autophagy is required for cellular homeostasis, eliminating defective ubiquitin-tagged proteins and organelles[16-19], clearing cell fate determinants and cell remodeling[20-22]. Defects in autophagy contribute to many disorders, including neurodegeneration[23], hepatomegaly[24] and aging[15,18].

Here we show that MB^{d}s accumulate in stem cells and are lost upon differentiation. They are selectively degraded by linking the NBR1 autophagic receptor to the Cep55 MB protein. MB^{d}s accumulate by evasion of autophagosome encapsulation, asymmetric inheritance, and maintenance of low autophagic activity. Reprogramming efficiency and *in vitro* tumorigenicity are increased following experimental elevation of MB^{d} levels suggesting non-mitotic roles for these organelles in stem and cancer cells.

RESULTS

Post-mitotic midbodies accumulate within cells

Multiple MB^{d}s were observed in subpopulations of cells by immunofluorescence (IF), but their precise location was unclear (up to 20; Fig. 1a, b). Three-dimensional reconstruction of immunofluorescent images revealed multiple MB^{d}s inside polarized and nonpolarized cells

(Fig. 1c, d). Immuno-electron microscopy confirmed this localization and revealed ultrastructural features characteristic of MB^{d}s[8,14] (Fig. 1e). About 70% of cell-associated MB^{d}s were trypsin-resistant, suggesting that they were intracellular (Fig. 1f). This intracellular localization of MB^{d}s suggested that they might accumulate in cells through successive divisions (below).

MB^{d}s were also released from cells. In 2-day co-cultures of HeLa cells stably expressing either monomeric RFP (cytoplasmic marker) or MKLP1-GFP (MB marker), about 7% of MKLP1-GFP+ MB^{d}s associated with RFP+ cells (Fig. 1g). Such free MB^{d}s were also generated by other cell types (e.g. human adult fibroblasts, HeLa; 1-10%). These observations resolve the conflict of previous studies suggesting that MB^{d}s are either retained and degraded[9,11,12] or released as remnants after abscission[8]. We show that MB^{d}s accumulate in some cells (Fig. 1a-d) but not others, and it is this cell type-specific difference in MB^d-accumulation that is the focus of this study.

MB^{d}s are inherited by the cell with the older centrosome

Multiple MB^{d}s often clustered around the centrosome or spindle pole (ref. 9 and data not shown), reminiscent of MB^d-sized aggresomes, which segregate to one daughter cell under control of centrosomes[25,26]. Moreover, centrosome age-dependent differences in signaling were observed late in cytokinesis[27]. These centrosome age-related differences led us to examine the relationship between centrosomes and MB^d inheritance.

In G1, the centrosome contains one mother centriole (MC) and one daughter centriole (DC)[3]. After centriole duplication, three generations of centrioles are present: an older mother, a younger mother and two new daughters[3,27]. The centrosome with the older MC is termed the older centrosome[4,5]. GFP-tagged centrin1 (CETN1-GFP)[28] expressed in mitotic HeLa cells was brightest at one of the four centrioles (92.2% of cells, n=116; Fig. 2a) and turned over very slowly (FRAP $t_{1/2}$ ~4 hours and ref. 5). The brightest centriole remained so from metaphase to late cytokinesis (91.3% of cells, n=46; supplementary information, Fig. S1a), suggesting that it was the older MC. This was confirmed by staining with the older centrosome marker, hCenexin1[27] (~90% of HeLa and MCF-7 cells, n=143 and n=347, respectively; Fig. 2b). Several other centriole antigens also showed intrinsic age-related differences in labeling (supplementary information, Fig. S1b).

Using CETN1-GFP to identify the older MC; bright-field imaging to follow MB dynamics in living cells; and immunofluorescence to confirm MB^d inheritance, we determined that MB^{d}s were preferentially inherited by the cell with the older centrosome. This was observed in pluripotent human embryonic stem cells (hESCs; 83.3% of H9, n=18; Fig. 2d), immortalized somatic cells (91.3% of hRPE-1, n=23) and cancer cells (U2OS: 84.6%, n=13; HeLa: 75.0%, n=24; Fig. 2c). We conclude that most inherited MB^{d}s are asymmetrically transferred to the daughter cell with the older centrosome in several cell types.

MB^{d}s accumulate in stem cells *in vivo*

Other studies have shown that the older centrosome is asymmetrically inherited by the stem cell during asymmetric divisions in the *Drosophila* male germline[4] and the mouse neocortex[5]. The association of the older centrosome with both MB^{d}s and stem cell divisions

led us to ask whether MB^ds were found in stem cell niches. To address this, we determined the localization of MB^ds in human and mouse tissues. In seminiferous tubules of testes, MB^ds were confined to the basal compartment, the site of germline stem cells and their mitotic progeny (both capable of self-renewal[29,30]) (Fig. 3a, up to 8 puncta/cell, 5-μm section). Electron microscopy also revealed multiple cytoplasmic structures with features characteristic of MB^ds within these cells (Fig. 3b, c).

In the ventricular zone (VZ, Sox2+[31]) of embryonic mouse brains, CD133-labeled MB^ds were associated with neural progenitors[13,14] (Fig. 3d and Supplementary information, Fig. S2). During asymmetric divisions, intracellular MB^ds were usually found in ventricle-facing daughter cells (progenitors; 75%, n=8) and not in daughters with presumed committed fates[5]. MB^ds in the human hair follicle were also confined to a subpopulation of cells in the stem cell niche, the bulge[32], suggesting distinct properties of this subpopulation (Fig. 3e, f). MB^ds were also enriched in β1–integrin+[33] mouse skeletal muscle progenitors (SMPs; 4-fold) over non-SMP cells. These observations suggested that MB^ds were selectively retained and accumulated during successive stem cell divisions *in vivo*.

MB^ds accumulate in stem cells *in vitro*

To rigorously test the idea that MB^ds are selectively inherited by stem cells, we examined MB^d fate during stem cell differentiation and somatic cell reprogramming. MB^d 'accumulation' was assessed by counting cells with >1 MB^d, as all cells can transiently acquire one MB^d after abscission (below). MB^d-accumulation decreased ~8-fold upon differentiation of hESCs (H1-OGN) to fibroblast-like cells (dH1f; Fig. 3g, h). Differentiation was judged by loss of embryonic stem cell markers (Oct4, Sox2, Klf4, Nanog) and gain of the CD13 differentiation marker[34,35]. In contrast, MB^d-accumulation increased ~7-fold after reprogramming dH1f cells to iPSCs[34,36] (dH1f-iPS; Fig. 3h, i). We conclude that MB^d-accumulation *in vitro* reflects that observed *in vivo*, and can be manipulated by altering the potency status of cells.

MB^d-accumulation is enhanced in tumor-derived cells

We next examined differences in MB^d-accumulation among cell lines derived from stem cells, normal dividing cells and cancer cells (Fig. 4a). MB^d-accumulation was low in primary and telomerase-immortalized normal cells and significantly higher in hESCs and iPSCs (~7-fold on average; Fig. 4a). Most cancer cells exhibited even higher levels of MB^d-accumulation. For example, MB^d-accumulation in tumorigenic MCF-10AT and MCF-10CA1a cells was much higher than in the normal MCF-10A parental line. The common ability of stem cells and cancer cells to accumulate MB^ds, express stem cell markers[37] and possess stem cell properties[38,39] suggests a relationship between MB^d-accumulation, tumorigenicity and cancer 'initiating' or 'stem' cells defined by the CSC theory[40].

MB^d-accumulation does not correlate with cell proliferation rate

A simple explanation for cell type-specific differences in MB^d-accumulation is variability in proliferation rates. Slower division rates could allow more time for MB^d degradation, as recently proposed[12]. However, we observed no correlation between population doubling-

time and MB^d-accumulation (Fig. 4a). It was still possible that MB^d-accumulating cells cycled faster than the bulk population. However, a cohort of cells pulse-labeled with EdU[41] showed a proportional decrease in EdU intensity, reflecting dilution of dye after successive divisions (Fig. 4b) and indicating that MB^d-accumulating and non-accumulating subpopulations had similar cycling rates (Fig. 4c, d).

MB^d-accumulating cells evade membrane encapsulation of MB^{d}s

We next asked if MB^{d}s occupied different sites within MB^d-rich and MB^d-poor cells. To test this, we used the Fluorescence Protease Protection (FPP) assay[42] to monitor degradation of MB^{d}s following plasma membrane permeabilization and protease addition (Fig. 5a). Under these conditions, MKLP1-GFP+ MB^{d}s were degraded in MB^d-rich HeLa cells but not in MB^d-poor hRPE-1 cells indicating that MB^d-poor cells sequestered MB^{d}s in membrane-bound compartments whereas MB^d-rich cells accumulated them in the cytoplasm (Fig. 5b). Importantly, the integrity of intracellular organelles was maintained during the course of these experiments (supplementary information, Fig. S3).

Stem cells and cancer cells evade lysosomal degradation of MB^{d}s

The protease resistance of MB^{d}s and low MB^d-accumulation in MB^d-poor hRPE-1 cells (Fig. 4a and 5b) suggested that MB^{d}s were delivered to a membrane-bound compartment for degradation, such as the lysosome. Indeed, MB^{d}s were often found within LAMP2[43]-labeled lysosomes in MB^d-poor cells (Fig. 5c). To test this further, we examined the fate of newly-formed MB^{d}s in synchronous populations of MB^d-poor cells (Fig. 5d). Three hours after release from mitosis, the percent of MB^d+ cells (MB^d levels) peaked at ~40% (50% being the maximum since half the cells were 'born' without a MB^d). This was followed by a peak in MB^d localization to lysosomes (~42% at 7 hours; Fig. 5d) and then a decrease of MB^{d}s to baseline levels (16-19 hours; Fig. 5d). These data and the FPP data suggested that MB^{d}s in hRPE-1 cells entered the cytoplasm, moved into lysosomes and were degraded before the next cell cycle (Fig. 5b, d).

If lysosomes are involved in MB^d degradation, lysosomal inhibition should increase MB^d levels. Indeed, when lysosomal activity was inhibited in MB^d-poor hRPE-1 cells with either chloroquine or E64d/PepA protease inhibitors[44] MB^d levels (Fig. 5e) and the percent of MB^{d}s found within lysosomes (Fig. 5c) were elevated. In contrast, MB^d levels and the percent of MB^{d}s in lysosomes in MB^d-rich cells (hESC, MCF-7; Fig. 5c, e) were largely unaffected by lysosomal inhibition (see supplementary information, Fig. S4a). The modest increase in MB^d+ HeLa cells (Fig. 5e) was consistent with their modest MB^d-accumulating ability (Fig. 4a). We conclude that lysosomal degradation prevents MB^d-accumulation in MB^d-poor cells, but does not play a major role in MB^d-rich cells (e.g. stem cells, CSCs) thus allowing MB^{d}s to accumulate.

Autophagic degradation controls intracellular MB^d levels

To determine how MB^{d}s were directed to lysosomes, we explored pathways leading to lysosomal degradation. Reported autophagy levels in MCF-7 and DLD-1 cells[45,46] suggested a relationship between autophagy and MB^d fate. Low autophagy levels in MCF-7 cells resulting from a deficiency in the autophagy gene, *BECN1* (also known as *Atg6*)[45], are

consistent with high MB^d-accumulation (~26-fold over normal cells; Fig. 4a). High autophagy levels in DLD-1 cells[46] are consistent with low MB^d-accumulation (only ~1.8-fold over normal cells; Fig. 4a). In agreement with this trend was the presence of MB^ds in autophagosomes of MB^d-poor cells (Fig. 6a).

Experimental reduction of autophagy activity using MEFs from *Atg5*-deleted mice[19] or by siRNA-mediated depletion of Atg7, increased MB^d levels (Fig. 6b). Induction of autophagy by rapamycin and lithilum chloride treatment[47,48] in HeLa cells or by exogenous BECN1 expression in MCF-7 cells, decreased MB^d levels (Fig. 6c). These results demonstrated the role of autophagy in regulating MB^d levels in different cell types, and suggested an inverse relationship between autophagic activity and MB^d-accumulation. This inverse relationship was revealed in 12 cell lines by LC3-II[44,49] or p62[44,50,51]-based measurements of autophagic activity (Fig. 6d, e and supplementary information Fig. S4b). We conclude that MB^d levels are, in part, modulated by cell type/lineage-specific autophagy (Fig. 3g-i, 4a, 6d and 6e).

NBR1 is an autophagic receptor for MB^d-specific degradation

To test whether MB^d degradation involves non-specific or receptor-mediated autophagy pathways[15], we investigated the mammalian autophagic receptors, p62[50-52] and NBR1[53,54]. p62 is implicated in MB^d clearance[12], whereas NBR1 is untested. NBR1 and p62 localized to mitotic MBs and MB^ds (Fig. 7a, top, data not shown, and ref. 12), suggesting that MB^d degradation involves receptor-mediated autophagy. NBR1-silencing in HeLa cells increased MB^d levels to Atg7-silencing levels (Fig. 6b and 7b), suggesting that NBR1 is likely a major autophagic receptor for MB^d degradation. In contrast, *p62*-deletion[51] or siRNA-mediated p62 depletion had no detectable effect on MB^d levels (Fig. 7b, c) or NBR1 recruitment to MB^ds (Fig. 7a, bottom).

To date, no MB^d target(s) for autophagic degradation have been identified. Candidate-based screening revealed that endogenous NBR1 co-immunoprecipitated with the MB protein Cep55 in hRPE-1 cells (Fig. 7d). Cep55 over-expression increased MB^d levels (Fig. 7e) and the level of NBR1-negative MB^ds (Fig. 7f), presumably through NBR1 sequestration in the cytoplasm (Fig. 7g). This suggested a role of Cep55 in NBR1-mediated MB^d degradation. We propose that the Cep55/NBR1 interaction couples MB^ds to the autophagic machinery to control MB^d fate.

Cells enriched in MB^ds exhibit increased reprogramming efficiency

We next examined the functional consequences of manipulating MB^d levels. We first tested the role of MB^ds during reprogramming[34,35,55] in cells stably expressing NBR1-specific shRNAs (shNBR1) to increase MB^d levels over controls (shNT). MB^d levels increased ~1.8-fold in dH1f cells, ~1.5-fold in IMR90[55] embryonic fibroblasts, and ~1.9-fold in hFib2[34] adult fibroblasts. Under these conditions, iPSC colony formation increased significantly in all three cell types depleted of NBR1: dH1f cells (up to 8.7-fold, avg. 3.1±0.5-fold), IMR90 cells (up to 4.2-fold, avg. 3.4±0.8-fold; Fig. 8a, b and supplementary information Table. S1) and adult hFib2 cells (up to 2.5-fold, avg. 1.7±0.5-fold). Similar results were obtained with different batches of viruses, different combinations of reprogramming factors, and different

viral delivery systems (see Methods). Importantly, increased reprogramming following NBR1-depletion occurred without significant changes in global autophagic activity (dH1f; Fig. 8c) or cell proliferation rate (shNBR1: 27.3±2.5hrs; shNT: 26.8±4.5hrs; n=6), suggesting that NBR1 is selective for MB^d degradation.

Cancer cells enriched in MB^{d}s exhibit increased *in vitro* tumorigenicity

Because MB^{d}s selectively accumulate in stem cell niches, hESCs, and iPSCs, we reasoned that they may also accumulate in CSCs. On the basis of Hoechst 33343 extrusion, the side population (SP) of MCF-7 cells[56] was isolated. These putative CSCs showed a 7-fold increase in MB^d+ cells over the non-SP population (MP; Fig. 8d).

To directly address the role of MB^{d}s in cancer cells, MKLP1-GFP-expressing HeLa populations with high or low percentages of MB^d+ cells were isolated by FACS, and tested for anchorage-independent growth. Increased colony formation was observed in the "MB^d high" versus the "MB^d low" population, and colony formation increased with increasing MB^d levels (up to 4-fold; Fig. 8e). An increase in colony formation was also observed in MB^d-enriched HeLa cells (Fig. 8f, left) and mouse hepatocarcinoma cells (134-4; Fig. 8f, right) following NBR1-silencing. Results of all three strategies suggest that MB^{d}s in cancer cell subpopulations may contribute to their tumorigenic potential.

DISCUSSION

We have identified new roles for MB^{d}s outside their canonical function in cytokinesis. This work provides the first evidence for MB^d-accumulation in stem cells, hESCs and iPSCs *in vivo* and *in vitro*, and for dramatic MB^d reduction in differentiating progeny of stem cells. MB^{d}s appear to function in maintaining or enhancing the pluripotency of stem cells and the tumorigenicity of cancer cells.

Our findings suggest that MB^d loss that accompanies stem cell differentiation is mediated by autophagic degradation, resulting in selective elimination of MB^{d}s in differentiated cells but retention in germ or stem cells. This process is intriguingly similar to clearance of P granule components in committed somatic cells of *C. elegans*, which is also mediated by autophagy[57]. Moreover, P granules contain molecules required for cell fate specification[58], and MB^{d}s contain stem cell markers[13,14] and enhance cell fate conversion (present study). It is thus tempting to propose that MB^{d}s may serve as scaffolds for organizing cell fate determinants. Equally intriguing is the observation that essentially all cancer cells examined contain MB^d-accumulating subpopulations, making this a common intrinsic property of both stem cells and cancer cells. The observation that MB^d-enriched cancer subpopulations exhibit enhanced *in vitro* tumorigenicity is consistent with the CSC model for potentiation of tumorigenicity[37-40].

Our data identify two primary mechanisms for MB^d-accumulation. The first is asymmetric MB^d inheritance by the daughter cell with the older centrosome (Fig. 8g, top). In fly testes and mouse neocortex, the old centrosome segregates to the stem cell during asymmetric divisions and is accompanied by increased microtubule-anchoring ability[4-6]. MB^d inheritance could be facilitated through increased anchoring of microtubules to the older

centrosome, and increased microtubule binding to the MB^d in the daughter cell with the older centrosome. This would be consistent with the observed MB^d-accumulation in stem cells but not in their differentiated progeny. Despite the slower division rate of stem cells *in vivo*[59], MB^d-accumulation could still occur via this mechanism. However, our results also indicate that such asymmetry occurs in different cell types, suggesting that it may only be physiologically relevant in stem cells and CSCs.

Evasion of autophagic degradation is a second mechanism for MB^d-accumulation (Fig. 8g, bottom). This is exemplified by the inverse relationship between MB^d levels and autophagic activity, and by changes in MB^d levels with manipulation of autophagy levels. MB^d-accumulation can also be mediated by uncoupling receptor-mediated entry into the autophagy pathway, since depletion of the NBR1 autophagic receptor or over-expression of the corresponding ligand, Cep55, increases MB^d levels. In contrast, another known autophagic receptor, p62, does not appear to be involved in MB^d clearance (Fig. 7b, c). NBR1 and p62 can form a complex[53,60]; however, evidence suggests that they may act independently as autophagic receptors[53]. Thus, p62/NBR1 complex formation may not be a prerequisite for autophagic degradation. Since NBR1-silencing increases MB^ds to levels seen following inhibition of autophagy in HeLa cells (Fig. 6b and 7b), NBR1-mediated autophagic degradation likely represents a major pathway for selective MB^d elimination. However, it is still possible that other autophagic receptors and MB^d ligands may exist and contribute to MB^d degradation, even though Cep55 is the sole MB ligand for the NBR1 receptor identified thus far (Fig. 7d). In our model, Cep55 and NBR1 and perhaps other MB^d ligands and autophagy receptors, act as switches that control MB^d fate. Ongoing proteomic analyses may identify other molecules and pathways for MB^d degradation.

MB^d levels can be further increased in autophagy-compromised *Atg5*$^{-/-}$ MEFs when lysosome enzymes are inhibited (data not shown), suggesting that other degradative pathways may contribute to MB^d degradation. Chaperone-mediated autophagy (CMA)[15,61], which targets ~30% of cytosolic proteins and is upregulated upon compromised autophagy[62], is a potential candidate since multiple MB proteins contain CMA-targeting motifs (KFERQ-like motifs)[61]. The proteasome system is another major cellular degradation pathway[63] but it doesn't appear to play a role in MB^d degradation (supplementary information, Fig. S5).

Other non-degradative processes may also regulate MB^d levels. Even though elevated proliferation rate has been proposed as a factor hindering autophagic MB^d degradation and causing MB^d-accumulation in cancer and normal cells[12], we didn't observe such a correlation (Fig. 4a). Additional work is required to determine if MB^d-accumulation also requires selective sequestration of previously inherited (pre-existing) MB^ds, as suggested by selective accumulation of MB^ds in stem cells of the testes and lateral ventricle of the brain (Fig. 3a-d). Release of MB^ds has also been observed in chicken and mouse neural progenitors[13,14] and in human cells (ref. 8 and Fig. 1g), and may be another, possibly minor pathway for eliminating MB^ds (or for intercellular signaling[14]). Finally, ongoing work is addressing whether MB^ds are distributed to both daughters of stem cells during symmetric divisions as might be expected if MB^ds are essential for stem cell function.

In summary, our results demonstrate that MB^ds are more than the remnants of cytokinesis. Their fate is differentially controlled in different cell types and mediated by diverse pathways. The shared ability to accumulate MB^ds by stem cells and putative CSCs, and the striking impact on cellular phenotypes following manipulation of MB^d levels suggest that MB^ds perform important cell type-specific functions that remain to be discovered.

METHODS

Cell lines

hESC and iPSC lines include H1 (WA01), H9 (WA09), H1-OGN (Oct4-EGFP knock-in H1)[36], and dH1f-iPS[34], which is reprogrammed from dH1f cells differentiated from H1-OGN (HSCI at Children's Hospital Boston). Differentiated lines include hRPE-1 (Clontech), MCF-10A, adult human fibroblasts (PCS-201-012, ATCC), hFib2[34], IMR90 (CCL-186, ATCC), *ex vivo* C57BL/6 MEFs, GFP-LC3-expressing $Atg5^{-/-}$ and $Atg5^{+/+}$ MEFs[19], and $p62^{-/-}$ and $p62^{+/+}$ MEFs[51]. Cancer cell lines include DLD-1, HeLa, NCC-IT, PC-3, U2OS, SAOS-2, 134-4, MCF-7, MCF-10AT, and MCF-10CA1a. Mouse skeletal muscle progenitors (SMPs)[33] and *in vitro* activated T cells were isolated and stimulated following standard protocols. Cells were used within 4 (primary cultures) or 10 (established cell lines, hESCs, and iPSCs) passages. Cells expressing MKLP1-GFP, monomeric RFP and CETN1-GFP were created in the present study or ref. 28.

Immunofluorescence and Immunohistochemistry

Immunofluorescence was performed as described[9,13,64]. To label lysosomes and autophagosomes, cells were permeabilized with 0.05% saponin in blocking buffer (10% goat serum/PBS). Preparations for immunohistochemistry were fixed with 4% paraformaldehyde/0.5% glutaraldehyde via perfusion. Testes were processed and stained following 2-4hr post-fixation with 4% paraformaldehyde. MB-derived rings between spermatocyte syncytia[65] were observed if stained longer. Images were taken on a Zeiss Axioskop 2 microscope, a Zeiss Axiovert 200 microscope with PerkinElmer UltraView LAS spinning disc, or an Olympus BX-51 microscope. Images were processed and analyzed with MetaMorph (Molecular Devices) and Imaris (Bitplane Inc.).

Electron Microscopy

Conventional EM—Mouse tissue, fixed with 5% glutaraldehyde in 50 mM sodium cacodylate buffer (pH=7.4) for 30 min via perfusion, was diced into 1-mm cubes for 1-hr post-fixation at 4°C. Cubes were washed with cacodylate buffer, stained and embedded in Spi-pon/Araldite, and sectioned at 70-500 nm before staining with 25% uranyl acetate and Reynold's lead citrate. Images were taken on a Philips CM12 electron microscope with an Erlangshen CCD Camera (Gatan).

Immunogold EM—MCF-7 cells on coverslips were prepermeabilized for 60 sec with preperm buffer (80 mM PIPES, pH6.8, 0.5 mM EGTA, 1 mM MgCl, 0.5% Triton X-100), fixed with 4% paraformaldehyde for 10 min, labeled for MKLP1 for 1 hour, processed as described[66] using 12-nm gold-conjugated goat anti-rabbit IgG (Jackson ImmunoResearch) and embedded in Spi-pon/Araldite. 80-nm sections were cut, stained and viewed as above.

Time-lapse imaging

CETN1-GFP-expressing lines were grown on 35-mm MatTek dishes (MatTek Corp.) or coverslips before imaging[9]. H9 hESCs were seeded on matrigel-coated dishes overnight, then transduced with CETN1-GFP, and grown for >72 hours in complete mTeSR1 medium (Stemcell Technologies). The transduced cells were imaged every 15 min in phenol red-free D-MEM/F12 medium (Invitrogen) with mTeSR1 supplement and 10 mM HEPES, and stained to confirm MB^d inheritance. Duplicate dishes of transduced cells were stained for stem cell markers to ensure cell quality.

MB^d quantification

Quantification was based on the markers that: 1) labeled both mitotic MBs and MB^ds (MKLP1, mgcRACGAP, or Cep55); 2) labeled MBs differently than MB^ds (α-tubulin or Aurora B); 3) defined cell boundaries (α-tubulin or ZO-1). Because Cep55, MKLP1, and mgcRACGAP also label centrioles and spindle midzones, cells were co-stained with centrosome antibody (e.g. 5051), and a size threshold for MB/MB^ds (1 μm) was introduced to exclude non-MB^d structures. Structures with MB-specific or non-MB/MB^d labeling were excluded from MB^d counts. Cell counts: For hESCs, 5-11 colonies were imaged from triplicates in each experiment. For other cell types, random fields were imaged until n > 500 cells. Each dividing cell was considered one cell.

Doubling time calculations

Cells were seeded (1-1.5×10^5/60-mm dish), and total cell counts were taken by hemocytometer every 24 hours for 4 days. Alternatively, cells were seeded (2.5-5.0×10^3/ well, 96-well plates), and the absorbance from an MTS-based colorimetric assay (#G3582; Promega Corp.) was used to estimate cell counts every 24 hours. Timepoints vs. Log_{10}(avg. cell counts or absorbance at that timepoint) was plotted and the slope ascertained. $T_{1/2}$ = $Log_{10}(2)$/ slope. For some cell lines, both methods were used and gave similar results.

MB^d localization assays

Extracellular trypsin treatment—MKLP1-GFP-expressing HeLa cells grown in MatTek dishes were imaged every 3 min, and underwent no morphological changes upon replacement of media with PBS. After trypsin addition, GFP+ MB^ds were monitored for 60-90 min for intensity reduction (degradation) or detachment from cells (dissociation).

Co-culture assay—Equal numbers of monomeric RFP- or MKLP-GFP-expressing cells were seeded and co-cultured in 60-mm dishes with coverslips. Cells were stained 2 days later, and the percentage of GFP+ MB^ds associated with RFP+ cells was determined.

FPP assay—The FPP assay was carried out as reported[42] except cells were plated in MatTek dishes 24 hours before co-transfection of MKLP1-GFP and GAPDH-dsRed (Lipofectamine 2000, Invitrogen). Cells were permeabilized and then digested with proteinase K (50 μg ml^{-1}). Constructs labeling mitochondria, peroxisomes, ER and Golgi were used as controls.

Lysosome and proteasome assays

Cells at 70% confluency were incubated with chloroquine (200 μM/PBS; Sigma), E64d + pepstatin A (E64d/PepA) (10 μg ml^{-1}/DMSO each; Sigma)[44,51] or solvents alone (controls) for 22 hours before fixation. Lysosome inhibition was confirmed and visualized after 12-hour DQ-Red BSA (10 μl ml^{-1}; Invitrogen) incubation. Mitotic hRPE-1 cells were treated with proteasome inhibitors, MG132 (1 μM; Sigma) or lactacystin (50 μM; Sigma) 1 hour after replating.

Autophagy manipulation assays

MB^ds were quantified in >500 cells in triplicate unless otherwise noted.

Protein depletion—siRNAs targeting human Atg7[67], p62[12], NBR1[53] (2503-2521 bp, GenBank NM 005899), Lamin A/C[9], and GFP (5'-NNCAUGAAGCAGCACGACUUC-3') were Dharmacon. MB^d levels were analyzed 48 hours after 1-nmol siRNA transfection (Oligofectamine, Invitrogen). For NBR1 and p62 experiments, only cells negative for p62 and/or NBR1 immunofluorescence were analyzed.

Beclin1 (BECN1) overexpression—MB^d levels were analyzed in 265 Flag+ and 2200 control MCF-7 cells 48 hours after Flag-BECN1 (4 μg) or mock nucleofection (Amaxa).

LiCl + rapamycin treatment—MB^d levels in HeLa cells were examined 24 hours after treatment with LiCl (10 mM; Sigma) and rapamycin (200 nM; Calbiochem), or with DMSO.

CEP55-EGFP overexpression—MB^d levels and its NBR1-association were assessed in hRPE-1 cells (1×10^5/well, 6-well plates) 48 hours after CEP55-EGFP (1 μg), EGFP (1 μg) or mock transfection.

Biochemical assays

Protease and phosphatase inhibitors, cell lysates, SDS-PAGE and immunoblotting were purchased or carried out as described[9] unless specified.

Autophagy flux determination—Lysates of E64d/PepA (I) and DMSO (U) treated cells were blotted for α-tubulin and LC3. LC3-II levels were determined and normalized to α-tubulin using ImageJ. Autophagic flux = |100 – ((U/ I LC3-II level) × 100)|.

Immunoprecipitation—hRPE-1 cell lysates (50 mM Tris-HCl pH 7.5, 150 mM NaCl, 2 mM EDTA, 1 mM EGTA, 1% Triton X-100, 10% glycerol, 4°C) were pre-cleared for 1 hour with protein G-plus conjugated agarose beads (Santa Cruz) at 4°C, incubated with 2 μg normal IgG, anti-Cep55 or anti-NBR1 antibodies for 3 hours at 4°C, and incubated overnight at 4°C with 25 μl protein G-plus beads. Following washes with lysis buffer and elution, immunoprecipitated proteins were analyzed by SDS-PAGE and immunoblotting.

Assays for MB^d function

Cellular reprogramming—Viral production, transduction and reprogramming were performed as described[34,35,55,68]. Commercially-available shRNA against NBR1 (pSM2c-

shNBR1, V2MM_36901; 4-22 bp, GenBank NM 005899) was cloned into pGIPZ lentiviral vector (Open Biosystems). Embryonic fibroblasts (IMR90), adult fibroblasts (hFib2) and dH1f cells were transduced with either NBR1-specfic or non-targeting shRNA vector, and puromycin-selected to establish NBR1-depleted (shNBR1) and control (shNT) lines. dH1f (2.5×10^4/assay) were reprogrammed with lentiviral vectors[69] (Addgene #21162 and 21164) expressing *OCT4, SOX2, KLF4* and *c-MYC*[34,35,68] whereas the reprogramming of IMR90 and hFib2 cells (5×10^4/assay) also included lentiviral vectors expressing Nanog and Lin28[55,69] (Addgene #21163). iPSC colonies were quantified on day 21 based on Tra-1-60 expression using ImageJ, as reported[35,68], and with parameters: ≥148 (threshold), 0.5-1 (circularity), and either 10-infinity or 30-infinity (size).

Side Population (SP) assay—The assays were carried out as previously described[56] in MCF-7 cells. The MB^d levels in SP and non-SP populations were determined as described above.

Soft-agar assays—"MB^d high" and "MB^d low" subpopulations of MKLP1-GFP-expressing HeLa cells were separated by FACS, and plated in soft-agar (2.5×10^4/well, 6-well plates). The MB^d levels were determined 12-15 hours after plating aliquots of subpopulations onto coverslips. For the NBR1-silencing soft-agar assay, NBR1-depleted (shNBR1) and control (shNT) cells (1×10^5/100-mm dish) were plated. For both assays, cells were grown for ~3 weeks at 37°C, and stained as described[70]. Colonies were quantified microscopically, and the average from triplicate wells or plates presented.

Antibodies

Antibodies to the following proteins/tags were used in this study—Atg5 (1:2000, Cosmo Bio, CAC-TMD-PH-ATG); Atg7 (1:1000, ProSci, 3617); Actin (1:300, Sigma, AC-40); Aurora B (1:100, BD Trans Lab, 611082); CD13 (1:50, BioLegend, 301707); CD133 (1:200, eBioscience, 14-1331); Cep55 (1:50, 1:100 and 1:1000 for immunofluorescence, Abnova #H00055165-B01, Abnova #H00055165-A01, and the gift from K. Kurtche, respectively; 1:500 for immunoblotting, Genetax #GTX112190); hCenexin1 (1:100, a gift from K.S. Lee); Centriolin (1:200, ref. 9); Flag (1:200, Sigma, F7425); GAPDH (1:8000; Santa Cruz, SC-32233); GFP (1:1000; Abcam, ab6556 and Santa Cruz, sc-9996); GT335 (1:100; a gift from P. Denoulet); β1-Integrin (1:50; BD Phramingen); K15 (1:100; Lab Vision, MS-1068-P); LC3 (1:10 for immunofluorescence, Nano Tools, LC3-5F10; 1:300 for immunoblotting, Novus Bio NB100-2331); LAMP2 (1:50, H4B4 from DSHB); mgcRACGAP (1:500, Abcam, ab2270); MKLP1 (1:1000 for immunofluorescence, 1:200 for immunohistochemistry, 1:10 for immuno-EM, Santa Cruz, sc-867); NBR1 (1:500, Abnova, H00004077-B01P); p62, human samples (1:500, BD Trans Lab, 610833); p62, mouse samples (1:1000, Progen, GP62-C); RFP (1:200, Clontech, 632496); Na-K-ATPase (1:15, α6F from DSHB); α-tubulin (1:100 for immunofluorescence, 1:400 for immunoblotting, Sigma, T9026a; 1:100 for immunofluorescence, Millipore, CBL270); α-tubulin-FITC (1:300, Sigma, F2168); Tra-1-60-biotin (1:200, eBioscience, 13-8863); Ubiquitin (1:2000, BD BioSci, #550944); WGA-Alexa Fluor 555 (1:200, Molecular Probes, W32464); ZO-1-FITC (1:50, Zymed, 33-9111).

Statistics

Data was analyzed by Student's one-tailed paired *t*-test or unpaired with Welch's correction unless specified. One-way ANOVA was used in conjunction with Tukey's test for comparisons among multiple groups. For the EdU-labeling assay, the EdU intensity was first logarithmically transformed for the use of one-way ANOVA. Statistically analyzed experiments were completed at least 3 times.

Supplementary Material

Refer to Web version on PubMed Central for supplementary material.

Acknowledgments

We thank E. Baehrecke for critical reading of the manuscript, T. Schlaeger and colleagues for assistance with H1-OGN and associated cell lines, the UMMS Flow Facility for assistance with MB^{d}-enrichment, P. Furcinitti of UMMS Digital Light Microscopy Core Facility for assistance with imaging, the UMMS DERC Morphology Core for assistance with immunohistochemitry, D. Guertin and C. Sparks for assistance with SMP preparation, S. Lyle and C. Powers for sample preparation, and H-L. Liu for assistance with clone construction. We thank N. Mizushima for GFP-LC3 expressing, *Atg5*$^{-/-}$, and matched wild-type MEFs, M. Komatsu and T. Ishii for *p62*$^{-/-}$ and matched wild-type MEFs, S. Jones for *ex vivo* C57BL/6 MEFs, B. Lewis for mouse hepatocellular cancer lines, S. Pino for *in vitro* activated T cells, W. Jiang for MKLP1-GFP plasmid, K. Khanna for CEP55-EGFP plasmid, J. Lippincott-Schwartz and G. Gaietta for plasmids for FPP assay, B. Levine (UT Southwestern) for Flag-tagged BECN1 expressing plasmid, A. Khodjakov for CETN1-GFP expressing plasmids, K. Lee for hCenexin1 antibody and the Progeria Society for cell lines. The α6F antibody to Na-K-ATPase developed by D.M. Fambrough, and H4B4 antibody to LAMP2 developed by J.T. August and J.E.K. Hildreth were obtained from the Developmental Studies Hybridoma Bank developed under the auspices of the NICHD and maintained by The University of Iowa, Department of Biology, Iowa City, IA 52242. This work was supported by funding from the National Institutes of Health (GM051994) to S.J.D and (F32 GM084660-02) to D.M.B, the W.M. Keck Foundation to S.J.D., the Ellison Foundation (AG-SS-1918-07) to S.J.D., the Department of Defense (W81XWH-08-1-0457) to S.J.D. and (W81XWH-06-1-0140) to C-T. Chen, and the Diabetes and Endocrine Resource Center (5P30DK3252025). Core resources supported by the Diabetes Endocrinology Research Center grant DK32520 were also used (DK32520).

References

1. Eggert US, Mitchison TJ, Field CM. Animal cytokinesis: from parts list to mechanisms. Annu Rev Biochem. 2006; 75:543–66. [PubMed: 16756502]
2. Neumüller RA, Knoblich JA. Dividing cellular asymmetry: asymmetric cell division and its implications for stem cells and cancer. Genes Dev. 2009; 23:2675–99. [PubMed: 19952104]
3. Doxsey S, McCollum D, Theurkauf W. Centrosomes in cellular regulation. Annu Rev Cell Dev Biol. 2005; 21:411–34. [PubMed: 16212501]
4. Yamashita YM, Mahowald AP, Perlin JR, Fuller MT. Asymmetric inheritance of mother versus daughter centrosome in stem cell division. Science. 2007; 315:518–21. [PubMed: 17255513]
5. Wang X, et al. Asymmetric centrosome inheritance maintains neural progenitors in the neocortex. Nature. 2009; 461:947–55. [PubMed: 19829375]
6. Yamashita YM, Jones DL, Fuller MT. Orientation of asymmetric stem cell division by the APC tumor suppressor and centrosome. Science. 2003; 301:1547–50. [PubMed: 12970569]
7. Barr FA, Gruneberg U. Cytokinesis: placing and making the final cut. Cell. 2007; 131:847–60. [PubMed: 18045532]
8. Mullins JM, Biesele JJ. Terminal phase of cytokinesis in D-98s cells. J Cell Biol. 1977; 73:672–84. [PubMed: 873994]
9. Gromley A, et al. Centriolin anchoring of exocyst and SNARE complexes at the midbody is required for secretory-vesicle-mediated abscission. Cell. 2005; 123:75–87. [PubMed: 16213214]
10. Steigemann P, et al. Aurora B-mediated abscission checkpoint protects against tetraploidization. Cell. 2009; 136:473–84. [PubMed: 19203582]

11. Goss JW, Toomre DK. Both daughter cells traffic and exocytose membrane at the cleavage furrow during mammalian cytokinesis. J Cell Biol. 2008; 181:1047–54. [PubMed: 18573914]
12. Pohl C, Jentsch S. Midbody ring disposal by autophagy is a postabscission event of cytokinesis. Nat Cell Biol. 2009; 11:65–70. [PubMed: 19079246]
13. Marzesco AM, et al. Release of extracellular membrane particles carrying the stem cell marker prominin-1 (CD133) from neural progenitors and other epithelial cells. J Cell Sci. 2005; 118:2849–58. [PubMed: 15976444]
14. Dubreuil V, et al. Midbody and primary cilium of neural progenitors release extracellular membrane particles enriched in the stem cell marker prominin- 1. J Cell Biol. 2007; 176:483–95. [PubMed: 17283184]
15. Mizushima N, Levine B, Cuervo AM, Klionsky DJ. Autophagy fights disease through cellular self-digestion. Nature. 2008; 451:1069–75. [PubMed: 18305538]
16. Mizushima N, Klionsky D. Protein turnover via autophagy: implications for metabolism. Annu Rev Nutr. 2007; 27:19–40. [PubMed: 17311494]
17. Yorimitsu T, Klionsky DJ. Eating the endoplasmic reticulum: quality control by autophagy. Trends Cell Biol. 2007; 17:279–85. [PubMed: 17481899]
18. Levine B, Kroemer G. Autophagy in the pathogenesis of disease. Cell. 2008; 132:27–42. [PubMed: 18191218]
19. Kuma A, et al. The role of autophagy during the early neonatal starvation period. Nature. 2004; 432:1032–6. [PubMed: 15525940]
20. Fimia GM, et al. Ambra1 regulates autophagy and development of the nervous system. Nature. 2007; 447:1121–5. [PubMed: 17589504]
21. Tsukamoto S, et al. Autophagy is essential for preimplantation development of mouse embryos. Science. 2008; 321:117–20. [PubMed: 18599786]
22. Cecconi F, Levine B. The role of autophagy in mammalian development: cell makeover rather than cell death. Dev Cell. 2008; 15:344–57. [PubMed: 18804433]
23. Hara T, et al. Suppression of basal autophagy in neural cells causes neurodegenerative disease in mice. Nature. 2006; 441:885–9. [PubMed: 16625204]
24. Komatsu M, et al. Impairment of starvation-induced and constitutive autophagy in Atg7-deficient mice. J Cell Biol. 2005; 169:425–34. [PubMed: 15866887]
25. Rujano MA, et al. Polarised asymmetric inheritance of accumulated protein damage in higher eukaryotes. PLoS Biol. 2006; 4:2325–2335.
26. Johnston JA, Illing ME, Kopito RR. Cytoplasmic dynein/dynactin mediates the assembly of aggresomes. Cell Motil Cytoskeleton. 2002; 53:26–38. [PubMed: 12211113]
27. Anderson CT, Stearns T. Centriole age underlies asynchronous primary cilium growth in mammalian cells. Curr Biol. 2009; 19:1498–502. [PubMed: 19682908]
28. Piel M, Meyer P, Khodjakov A, Rieder CL, Bornens M. The respective contributions of the mother and daughter centrioles to centrosome activity and behavior in vertebrate cells. J Cell Biol. 2000; 149:317–30. [PubMed: 10769025]
29. Oatley JM, Brinster RL. Regulation of spermatogonial stem cell self-renewal in mammals. Annu Rev Cell Dev Biol. 2008; 24:263–86. [PubMed: 18588486]
30. Barroca V, et al. Mouse differentiating spermatogonia can generate germinal stem cells in vivo. Nat Cell Biol. 2009; 11:190–6. [PubMed: 19098901]
31. Bilgüvar K, et al. Whole-exome sequencing identifies recessive WDR62 mutations in severe brain malformations. Nature. 2010; 467:207–10. [PubMed: 20729831]
32. Morris RJ, et al. Capturing and profiling adult hair follicle stem cells. Nat Biotechnol. 2004; 22:411–7. [PubMed: 15024388]
33. Conboy MJ, Cerletti M, Wagers AJ, Conboy IM. Immuno-analysis and FACS sorting of adult muscle fiber-associated stem/precursor cells. Methods Mol Biol. 2010; 621:165–73. [PubMed: 20405366]
34. Park IH, et al. Reprogramming of human somatic cells to pluripotency with defined factors. Nature. 2008; 451:141–6. [PubMed: 18157115]

35. Chan EM, et al. Live cell imaging distinguishes bona fide human iPS cells from partially reprogrammed cells. Nat Biotechnol. 2009; 27:1033–7. [PubMed: 19826408]
36. Zwaka TP, Thomson JA. Homologous recombination in human embryonic stem cells. Nat Biotechnol. 2003; 21:319–21. [PubMed: 12577066]
37. Visvader JE, Lindeman GJ. Cancer stem cells in solid tumours: accumulating evidence and unresolved questions. Nat Rev Cancer. 2008; 8:755–68. [PubMed: 18784658]
38. O'Brien CA, Pollett A, Gallinger S, Dick JE. A human colon cancer cell capable of initiating tumour growth in immunodeficient mice. Nature. 2007; 445:106–10. [PubMed: 17122772]
39. Pece S, et al. Biological and molecular heterogeneity of breast cancers correlates with their cancer stem cell content. Cell. 2010; 140:62–73. [PubMed: 20074520]
40. Pardal R, Clarke MF, Morrison SJ. Applying the principles of stemcell biology to cancer. Nat Rev Cancer. 2003; 3:895–902. [PubMed: 14737120]
41. Salic A, Mitchison TJ. A chemical method for fast and sensitive detection of DNA synthesis in vivo. Proc Natl Acad Sci U S A. 2008; 105:2415–20. [PubMed: 18272492]
42. Lorenz H, Hailey DW, Lippincott-Schwartz J. Fluorescence protease protection of GFP chimeras to reveal protein topology and subcellular localization. Nat Methods. 2006; 3:205–10. [PubMed: 16489338]
43. Eskelinen EL, Tanaka Y, Saftig P. At the acidic edge: emerging functions for lysosomal membrane proteins. Trends Cell Biol. 2003; 13:137–45. [PubMed: 12628346]
44. Klionsky DJ, et al. Guidelines for the use and interpretation of assays for monitoring autophagy in higher eukaryotes. Autophagy. 2008; 4:151–75. [PubMed: 18188003]
45. Liang XH, et al. Induction of autophagy and inhibition of tumorigenesis by beclin 1. Nature. 1999; 402:672–6. [PubMed: 10604474]
46. Sato K, et al. Autophagy is activated in colorectal cancer cells and contributes to the tolerance to nutrient deprivation. Cancer Res. 2007; 67:9677–84. [PubMed: 17942897]
47. Sarkar S, et al. A rational mechanism for combination treatment of Huntington's disease using lithium and rapamycin. Hum Mol Genet. 2008; 17:170–8. [PubMed: 17921520]
48. Sarkar S, et al. Lithium induces autophagy by inhibiting inositol monophosphatase. J Cell Biol. 2005; 170:1101–11. [PubMed: 16186256]
49. Mizushima N, Yoshimori T. How to interpret LC3 immunoblotting. Autophagy. 2007; 3:542–5. [PubMed: 17611390]
50. Bjorkoy G, et al. p62/SQSTM1 forms protein aggregates degraded by autophagy and has a protective effect on huntingtin-induced cell death. J Cell Biol. 2005; 171:603–14. [PubMed: 16286508]
51. Komatsu M, et al. Homeostatic levels of p62 control cytoplasmic inclusion body formation in autophagy-deficient mice. Cell. 2007; 131:1149–63. [PubMed: 18083104]
52. Pankiv S, et al. p62/SQSTM1 binds directly to Atg8/LC3 to facilitate degradation of of ubiquitinated protein aggregates by autophagy. J Biol Chem. 2007; 282:24131–45. [PubMed: 17580304]
53. Kirkin V, et al. A role for NBR1 in autophagosomal degradation of ubiquitinated substrates. Mol Cell. 2009; 27:505–16. [PubMed: 19250911]
54. Waters S, et al. Interactions with LC3 and polyubiquitin chains link nbr1 to autophagic protein turnover. FEBS Lett. 2009; 583:1846–52. [PubMed: 19427866]
55. Yu J, et al. Induced pluripotent stem cell lines derived from human somatic cells. Science. 2007; 318:1917–20. [PubMed: 18029452]
56. Engelmann K, Shen H, Finn OJ. MCF7 side population cells with characteristics of cancer stem/progenitor cells express the tumor antigen MUC1. Cancer Res. 2008; 68:2419–26. [PubMed: 18381450]
57. Zhang Y, et al. SEPA-1 mediates the specific recognition and degradation of P granule components by autophagy in *C. elegans*. Cell. 2009; 136:308–21. [PubMed: 19167332]
58. Strome S. Specification of the germ line. WormBook. 2005; 28:1–10. [PubMed: 18050414]
59. Fuchs E. The tortoise and the hair: slow-cycling cells in the stem cell race. Cell. 2009; 137:811–9. [PubMed: 19490891]

60. Lamark T, et al. Interaction codes within the family of mammalian Phox and Bem1p domain-containing proteins. J Biol Chem. 2003; 278:34568–81. [PubMed: 12813044]
61. Majeski AE, Dice JF. Mechanisms of chaperone-mediated autophagy. Int J Biochem Cell Biol. 2004; 36:2435–44. [PubMed: 15325583]
62. Kaushik, et al. Constitutive Activation of Chaperone-mediated Autophagy in Cells with Impaired Macroautophagy. Mol Biol Cell. 2008; 19:2179–92. [PubMed: 18337468]
63. Nedelsky N, et al. Autophagy and the ubiquitin-proteasome system: collaborators in neuroprotection. Biochim Biophys Acta. 2008; 1782:691–9. [PubMed: 18930136]
64. Xu P, Davis RJ. c-Jun NH2-terminal kinase is required for lineagespecific differentiation but not stem cell self-renewal. Mol Cell Biol. 2010; 30:1329–40. [PubMed: 20065035]
65. Greenbaum MP, Ma L, Matzuk MM. Conversion of midbodies into germ cell intercellular bridges. Dev Biol. 2007; 305:389–96. [PubMed: 17383626]
66. Mitchison T, Evans L, Schulze E, Kirschner M. Sites of microtubule assembly and disassembly in the mitotic spindle. Cell. 1986; 45:515–27. [PubMed: 3708686]
67. Yu L, et al. Regulation of an ATG7-beclin 1 program of autophagic cell death by caspase-8. Science. 2004; 304:1500–2. [PubMed: 15131264]
68. Loewer S, et al. Large intergenic non-coding RNA-RoR modulates reprogramming of human induced pluripotent stem cells. Nat Genet. 2010; 42:1113–7. [PubMed: 21057500]
69. Yu J, et al. Human induced pluripotent stem cells free of vector and transgene sequences. Science. 2009; 324:797–801. [PubMed: 19325077]
70. Sachdev S, Bu Y, Gelman IH. Paxillin-Y118 phosphorylation contributes to the control of Src-induced anchorage-independent growth by FAK and adhesion. BMC Cancer. 2009; 12(9):12. [PubMed: 19138410]

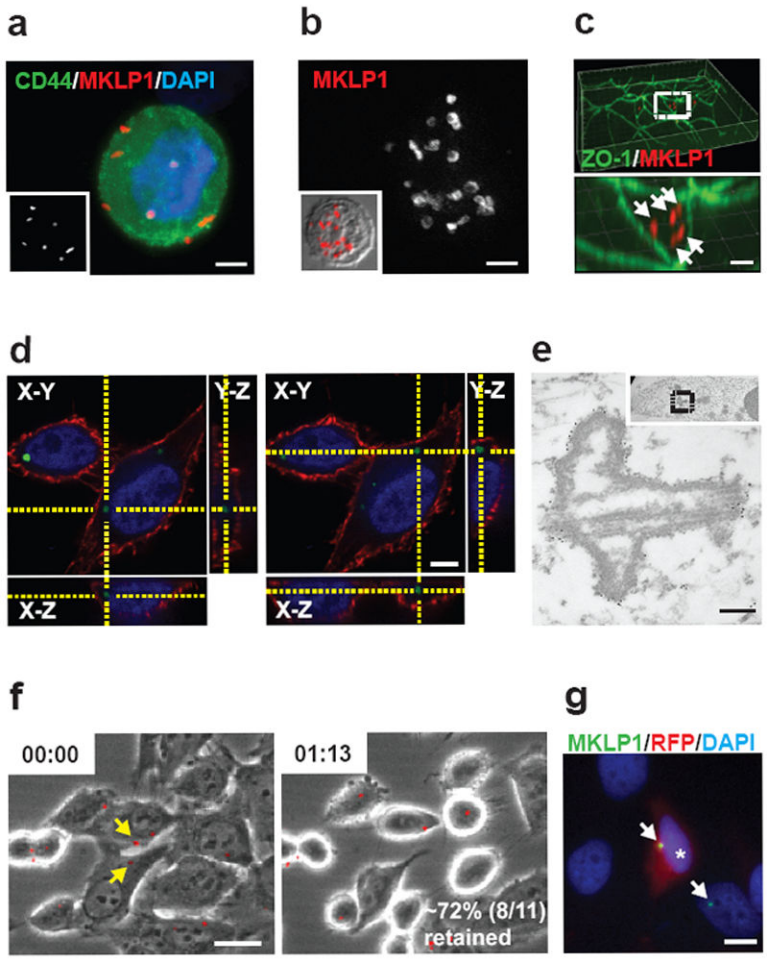

Figure 1.

MB^{d}s accumulate within cells. (**a, b**) Multiple MB^{d}s associate with a PC3 cell (a) and a B-lymphoblast (b). Insets (a) MB^{d} labeling and (b) merged phase-contrast image with MB^{d} labeling to show cell boundaries. MKLP1, MB^{d} marker (a, b; red); CD44, membrane (a; green); DAPI, DNA (a; blue). Bar, 5 μm (a) and 2 μm (b). (**c, d**) Three-dimensional reconstruction of polarized cells in a monolayer (c) and a HeLa cell (d) show intracellular MB^{d}s. (c) ZO-1, tight junction; MKLP1, MB^{d}s. Bar, 2 μm. Enlargement (c, bottom) of box (c, top) shows five MB^{d}s (arrows). (d) Wheat germ agglutinin, plasma membrane (red); MKLP1-GFP, MB^{d}s (green); DAPI, DNA (blue). Bar, 5 μm. (**e**) Electron micrograph of a MB^{d} in a permeabilized MCF-7 cell showing immungold labeling with MKLP1 antibodies. Inset, lower magnification of the MB^{d} (boxed) in cell; nucleus, right. Bar, 200 nm. (**f**) Time-lapse images during extracellular trypsin treatment of HeLa cells show retention of most MB^{d}s (MKLP1-GFP, red). Two MB^{d}s (yellow arrows) are lost upon treatment, suggesting digestion and/or dissociation. Time (hr:min) post-trypsin. Bar, 5 μm. (**g**) Two-day co-cultures of HeLa cell expressing either MKLP1-GFP (MB^{d} marker) or cytosolic RFP. Green MB^{d}s (arrows) associated with red cells (asterisk) indicate post-mitotic transfer of MB^{d}s between cells. Bar, 10 μm.

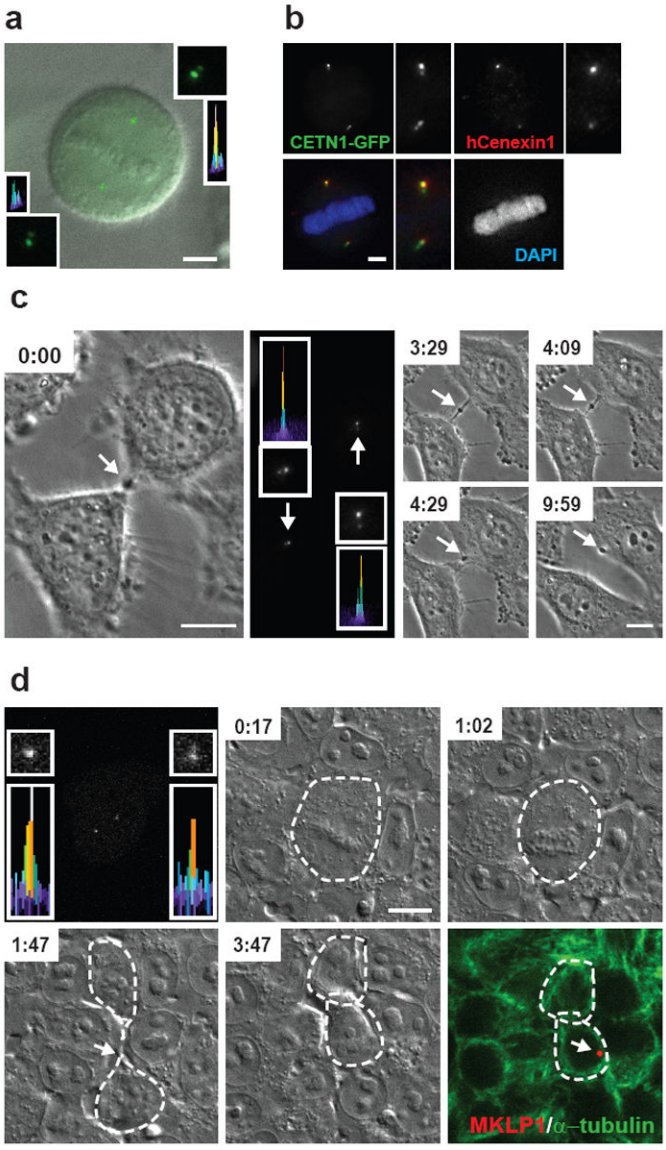

Figure 2.

MB[d]s are preferentially inherited by the cell with the older centrosome. (**a**) CETN1-GFP signal is brighter in upper centrosome/spindle pole of a mitotic spindle. The merged DIC image with CETN1-GFP labeling at two centrosomes shows metaphase chromosome. Insets (lower left, upper right), enlargement and semi-quantitative integrated intensity profile of centrioles. Bar, 5 μm. (**b**) The brighter CETN1-GFP signal represents the older centrosome as it co-stains more intensely for hCenexin1 and remains more intense throughout cell division (supplementary information, Fig. S1a). Bar, 5 μm. Lower left, merge. (**c, d**) Time-lapse images show that the mitotic MB is preferentially inherited by the daughter cell with the older centrosome in HeLa cells (c) and hESCs (d). Cells were imaged at the indicated times (hr:min) from telophase by phase-contrast microscopy (c) and from metaphase by DIC microscopy (d). Middle panel of (c) and left panel of (d), CETN1-GFP at centrosomes; enlargements and integrated intensity profiles show the daughter cell having the older

centrosome (c, upper; d, lower) inherits the MB^d (Time-lapse images: 9:59 in c; lower right image in d). Mitotic MB and MB^ds (c, d; arrows). MKLP1, MB^d marker (red); α-tubulin, mitotic MB and cell boundary marker (green); DAPI, DNA (blue). Bars, 10 μm (c, d).

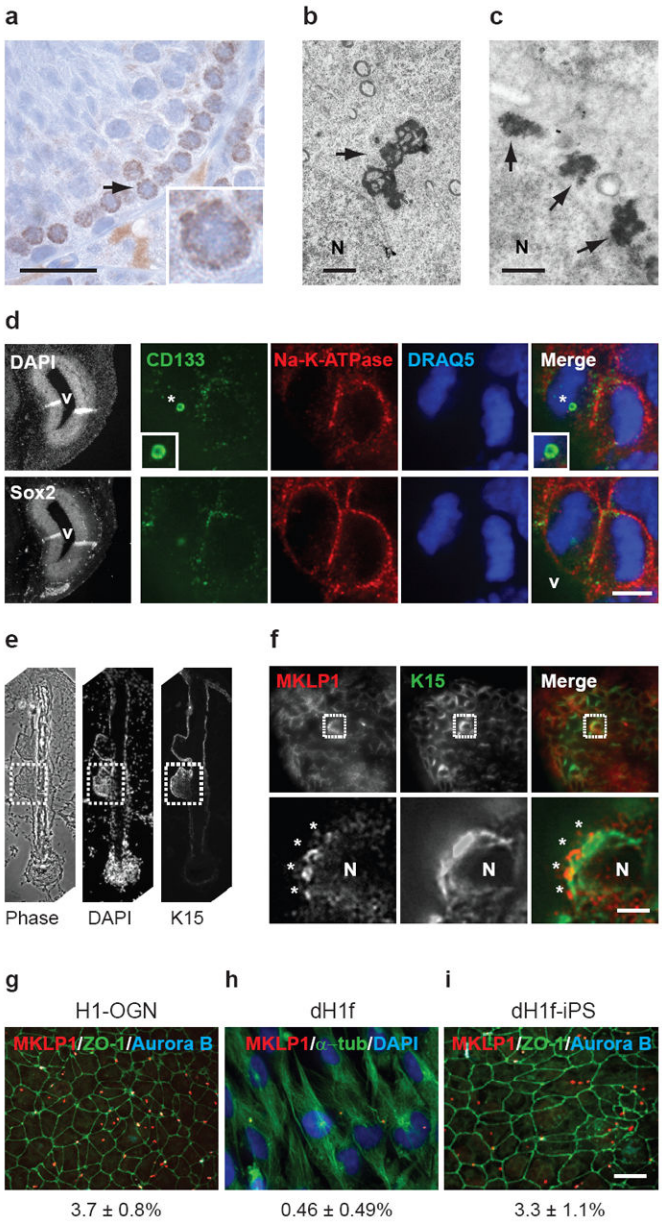

Figure 3.

MB^{d}s accumulate in stem cells *in vivo* and *in vitro*. (**a**) Histological section through mouse seminiferous tubules labeled for MKLP1 shows several MKLP1+ puncta in cells of the basal layer where stem cells reside. Bar, 20 μm. Inset, enlargement of the cell (arrow) (**b, c**) Electron micrographs of mitotic MB (b, arrow) and multiple MB-like structures in interphase cells with similar shape and size in a juxtanuclear position (c, arrows) in basal cells of mouse seminiferous tubules. N, nucleus. Bars, 1 μm. (**d**) Representative planes of a neural progenitor cell in the ventricular zone (Sox2+, left-bottom panel) of an E13.5 mouse brain show that an intracellular MB^d (asterisk) is associated with the ventricle-facing daughter in the asymmetrically dividing cell (top row). The bottom row emphasizes the position of paired chromosomes in a dividing anaphase cell. CD133, MB/MB^d marker

(green); Na-K-ATPase, cell-border marker (red); DRAQ5, DNA (blue); DAPI, DNA. Ventricle (V). Bar, 5 μm. Note that abscission occurs apically in these cells. (**e**) A histological section through a hair follicle (left, phase-contrast microscopy) stained for the stem cell marker keratin 15 to identify the bulge region (dotted box), the stem cell niche. DNA stain (DAPI) and the phase-contrast image show full follicle architecture. (**f**) Upper panels show MB^d-accumulating cells in the bulge region (boxed) colabeled with K15 and MKLP1. Enlargements (lower panels) of the boxed region highlight a cell with four MB^ds (asterisks). N, nucleus. Bar, 5 μm. (**g-i**) Quantitative analysis and representative images show a decrease in MB^d-accumulating cells upon the differentiation of pluripotent stem cells (g, H1-OGN) to fibroblast-like cells (h, dH1f), and an increase in MB^d-accumulating cells after reprogramming differentiated cells (h) to induced pluripotent stem cells (i, dH1f-iPS). (g-i) numbers refer to mean ± s.d., n=3. MKLP1, MB^ds; ZO-1, tight junctions; α-tubulin, microtubules; Aurora B, MBs. Bar, 10 μm.

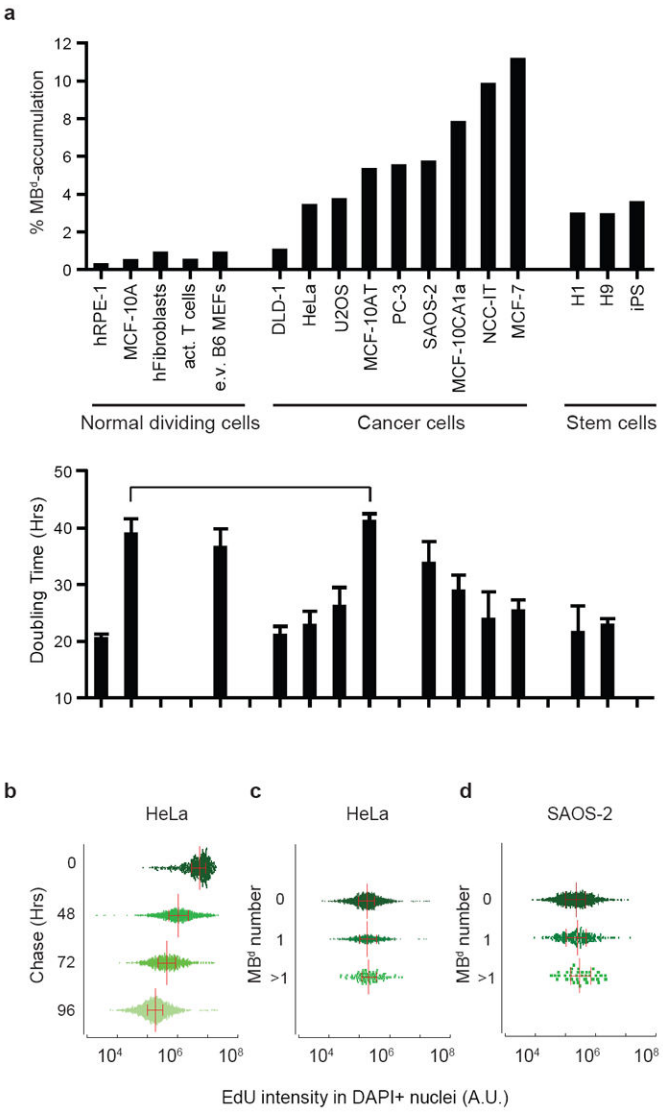

Figure 4.

MB^d-accumulation is high in stem cells and subpopulations of cancer cells and does not correlate with cell doubling time. (**a**) Percent of cells that accumulate MB^{d}s (>1) in a range of different cell types, as indicated. Below, doubling-times of representative cell lines aligned with MB^d-accumulation data. Data are presented as mean ± s.d.; Cell lines are examined in triplicate (MCF-10A, DLD-1, MCF-10AT, MCF-7, H1, and H9), or quadruplicate (e.v. B6 MEFs, HeLa, SAOS-2, and MCF-10CA1a), except hRPE-1 (n=6), U2OS (n=7) and NCC-IT (n=8). Horizontal line, cell lines with different MB^d-accumulation potential (14-fold) but similar doubling time. (**b**) Cells pulse-chased with EdU show a decrease in EdU intensity (x-axis) over time (y-axis), reflecting dilution of dye after cell divisions. (**c, d**) After a 96-hr chase period, EdU levels were compared between cells with MB^d numbers of >1, 1, and 0 (y-axis) in HeLa (c) and SAOS-2 cells (d). In both cases, no significant differences were noted (c, p=0.2101; d, p=0.5609, one-way ANOVA, with at least 800 cells analyzed for each experiment, n=3), indicating similar cycling rates among

different subpopulations of cells. (b-d) Each graph is a representative experiment. Cells analyzed shown by green points, median depicted by vertical red lines, and horizontal red lines with ticks illustrate the interquartile range.

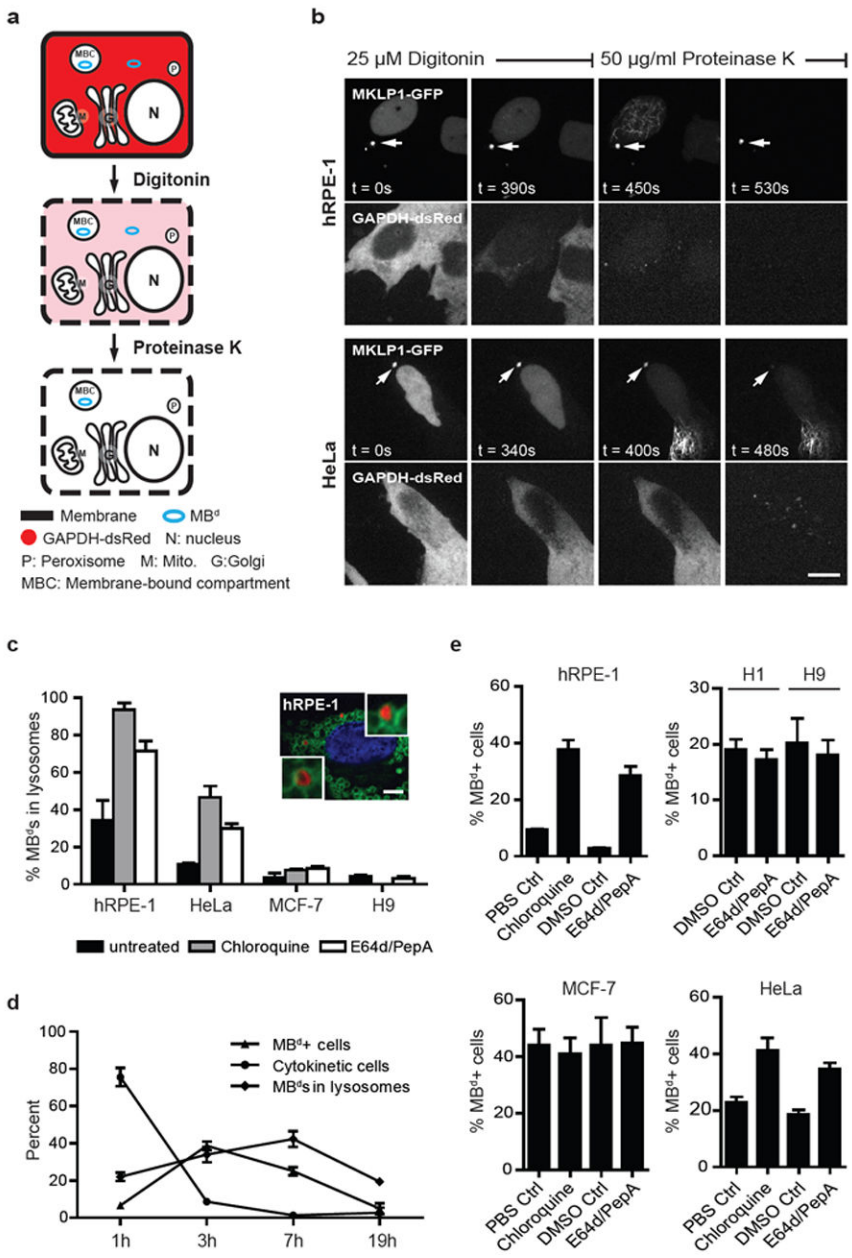

Figure 5.

MB^{d}s in stem and cancer cells evade membrane encapsulation and lysosomal degradation. (**a**) Depiction of fluorescence protease protection (FPP) assay. Digitonin selectively permeabilizes the plasma membrane but not internal membranes. Proteinase K degrades cytoplasmic components but membranous compartments remain intact. Under these conditions, MKLP1-GFP-labeled MB^{d}s (blue circle) in the cytoplasm will be degraded whereas those inside membrane-bound compartments (MBCs) will not. (**b**) MB^{d}s in MB^{d}-poor hRPE-1 cells are largely protected (~90% in membranous compartments, cells analyzed=10), whereas most MB^{d}s in HeLa cells are not (~27%, cells analyzed: 11), and are thus degraded in cytoplasm. Bar, 5 μm. (**c**) Graph depicting the presence of MB^{d}s in

lysosomes upon chloroquine or E64d/pepstatin A (E64d/PepA) inhibition in hRPE-1 and HeLa cells, but not in MCF-7 and H9 hESCs. Chloroquine treatment of H9 hESCs is not included as it caused differentiation and cell death. A representative image of hRPE-1 cells inhibited by chloroquine is shown depicting two MB^ds inside lysosomes. MKLP1 and LAMP2 are used as MB^d (red) and lysosome (green) markers, respectively. DAPI, DNA (blue). n=100 MB^ds/treatment in each of the biological triplicates. Bar, 5 μm. (**d**) Graph showing the percent of MB^d+ cells (MB^d levels), the percent of MB^ds within lysosomes, and the percent of cells exiting cytokinesis following synchronization. MKLP1 and LAMP2 are used as markers as in (c). Note that MB^ds are transferred into only one of the two nascent daughter cells after abscission (Fig. 2d), so a 50% maximum will be expected for MB^d+ cells. The peak of MB^ds transferred to cells is 3 hours after plating followed by a peak of MB^ds entering lysosomes at 7 hours. (**e**) Both chloroquine and E64d/PepA treatments increase the percent of MB^d+ cells in hRPE-1 cells and HeLa cells (chloroquine: p=0.0021 and p=0.0187, respectively; E64d/PepA: p=0.0022 and p=0.0043, respectively; n=3 for all experiments). In contrast, lysosomal inhibition has no detectable effect on hESCs (H1, H9) and MCF-7 cancer cells. Data are presented as mean ± s.d. (c-e), except mean ± s.e.m. in hESCs (e).

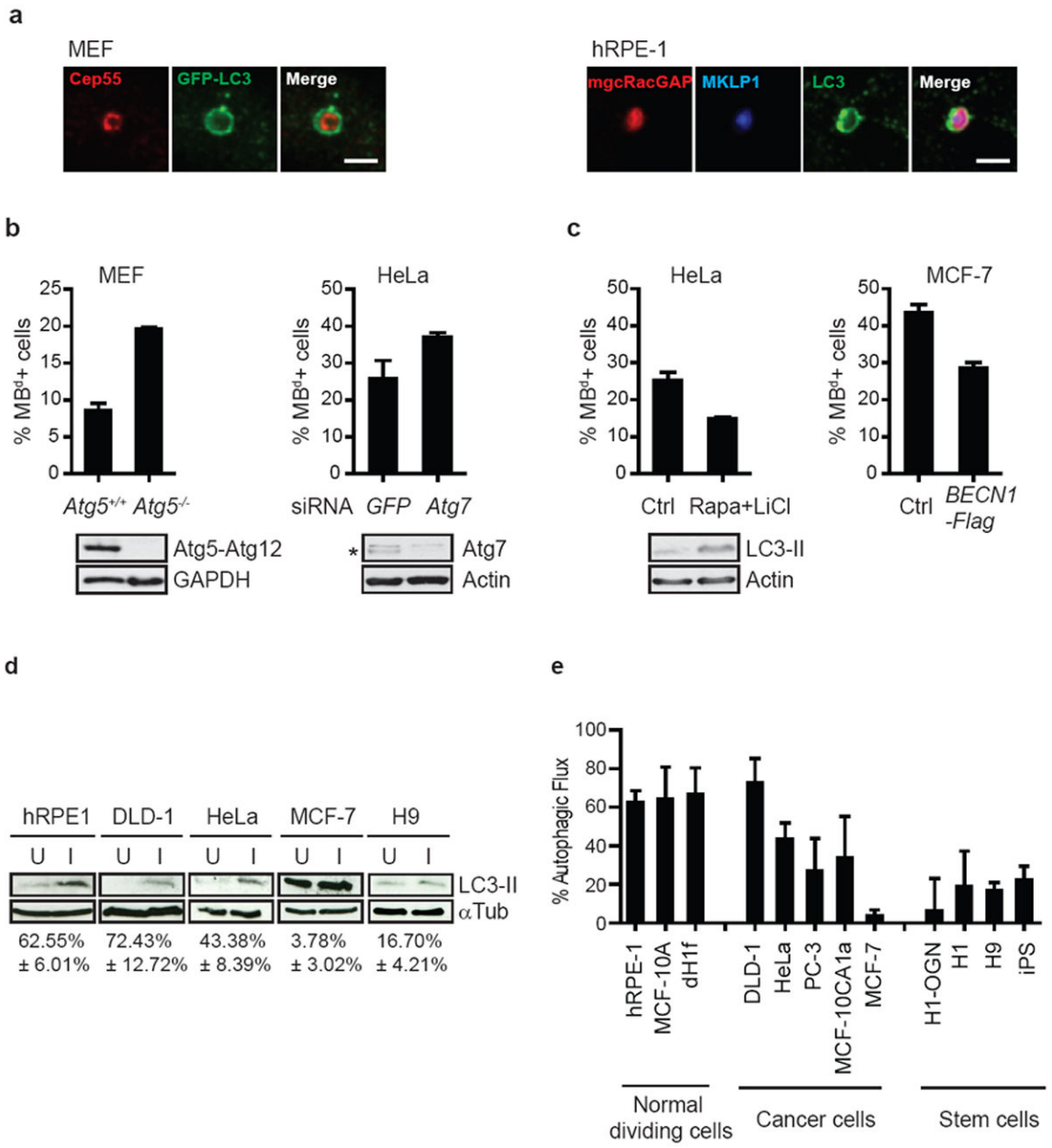

Figure 6.

Autophagy controls intracellular MB^d levels. (**a**) Single-plane confocal images of MB^{d}s within LC3-positive autophagosomes in MEFs expressing GFP-LC3 (left) and in hRPE-1 cells stained for endogenous LC3 (right). MB^d markers: Cep55, MKLP1, or mgcRACGAP. Autophagosomes: GFP-LC3 or LC3. Note that MKLP1 (blue) and mgcRACGAP (red) are co-localized (magenta) in the autophagosome (green), suggesting that MB^{d}s are sorted into autophagosomes. Bars, 2 μm. (**b**) Decreasing autophagy levels by deletion of *Atg5* gene (left, MEFs) or depletion of Atg7 by siRNA (right, HeLa) significantly increases the percent of MB^d+ cells (p=0.0019 and p=0.021, respectively, n=3). Immunoblots confirm loss of the Atg5-Atg12 conjugation in mutant cells and depletion of Atg7 (asterisk). (**c**) Rapamycin (Rapa) and lithium chloride (LiCl) co-treatment induces autophagy and decreases the

percent of MB^d+ cells (left, HeLa; p=0.0056, n=3). Immunoblots showing increased LC3-II levels confirm autophagy induction. Induction of autophagy by over-expression of Flag-tagged BECN1 reduces the percent of MB^d+ cells (right, MCF-7; p=0.0008, n=4) (**d**) Representative immunoblots showing high autophagy levels in normal cells and low levels in stem cells and cancer cells. Autophagic flux (autophagic activity) was measured by changes in the levels of LC3-II, in the presence or absence of lysosomal inhibitors E64d/PepA. U, uninhibited. I, inhibited. Below, the average of the percent change in LC3-II levels after lysosomal inhibition from 3 experiments. α-tubulin, loading control. (**e**) Quantification of autophagic flux from 3 experiments in different cell lines. Normal dividing cells (MB^d-poor) typically have high autophagic flux, whereas stem and cancer cells (MB^d-rich) have low autophagic flux. The data are presented as mean ± s.d. (b-e).

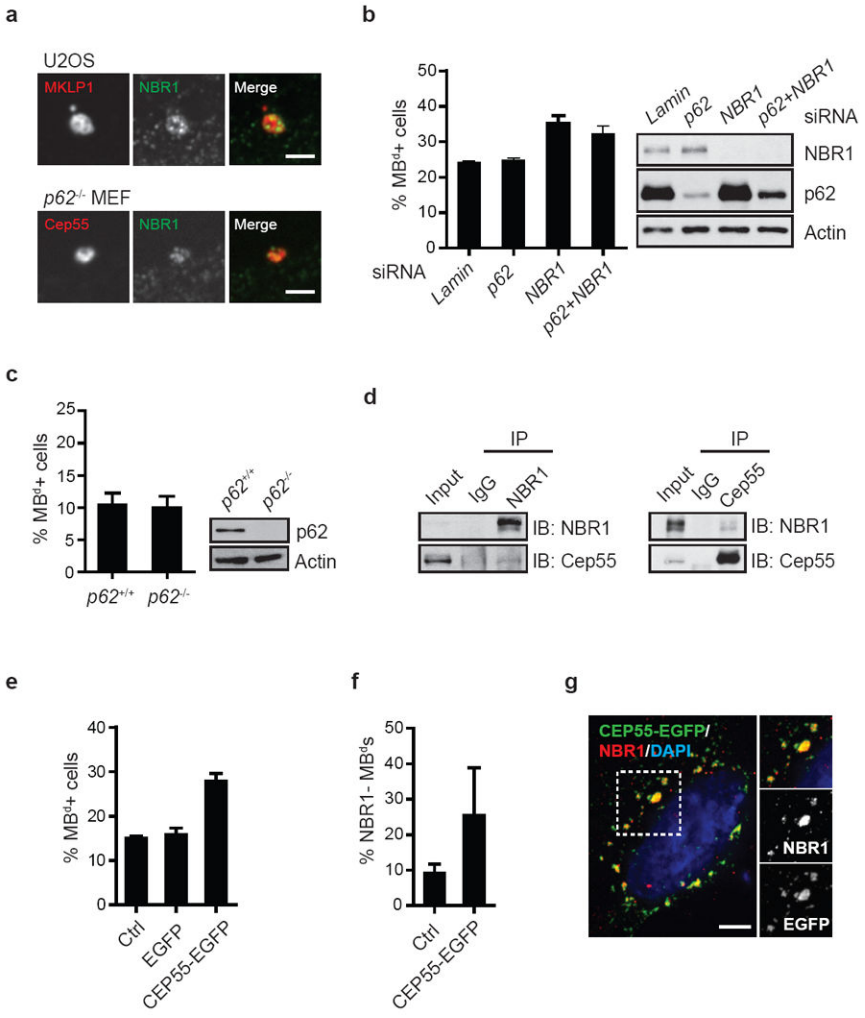

Figure 7.

NBR1 is a receptor for targeting MB^{d}s to the autophagy pathway. (**a**) Single-plane confocal images showing co-localization of the MB^{d} and the autophagic receptor, NBR1, in U2OS cells and *p62*-deleted MEFs. MB^{d} markers: MKLP1 or Cep55. Bar, 2 μm. (**b**) The percent of MB^{d}+ cells is significantly increased following the depletion of NBR1 (p=0.022, n=3), but not another autophagic receptor, p62. Co-depletion of NBR1 and p62 does not further increase MB^{d} levels over NBR1 depletion alone. (**c**) Deletion of the *p62* gene does not affect the percent of MB^{d}+ cells. For (b) and (c), immunoblots verify protein loss. (**d**) Co-immunoprecipitation reveals Cep55 and NBR1 form a complex. Precipitated proteins and 5% of the input material (Input) were analyzed by immunoblotting with antibodies against NBR1 or Cep55. (**e-g**) Over-expression of CEP55-EGFP increases the percent of MB^{d}+ cells (e; p=0.0007, n=3) and the percent of NBR1-negative MB^{d}s (f; p=0.0568, n=3), presumably by sequestering NBR1 (red) away from MB^{d}s in cells expressing CEP55-EGFP (green) as shown in (g), and consequently preventing MB^{d} degradation. The dotted box in (g) is enlarged (top right panel), and the labeling of NBR1 and CEP55-EGFP (middle and bottom right panel) are also presented. DAPI, DNA (blue). Bar, 5 μm. The data are presented as mean ± s.d. (b, c, e, and f).

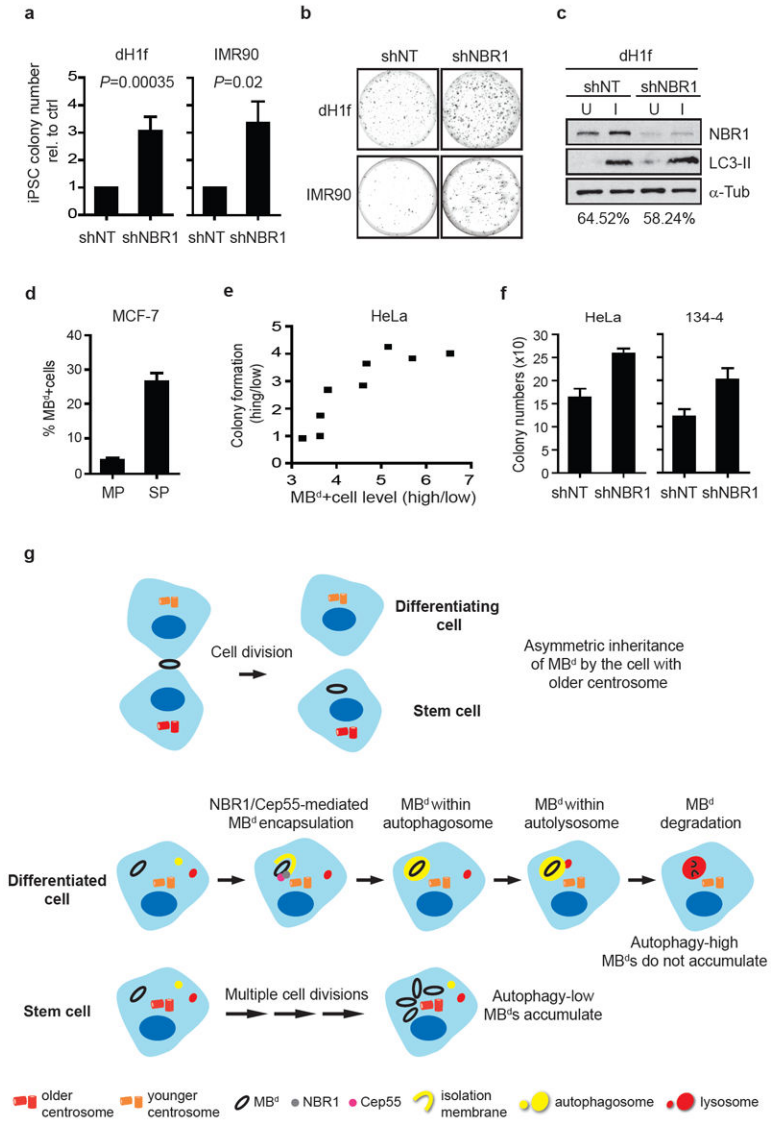

Figure 8.

MB^{d} enrichment increases reprogramming efficiency and enhances *in vitro* tumorigenicity. (**a-c**) Reprogramming is more efficient after MB^{d} enrichment. Differentiated cells (dH1f) and embryonic fibroblasts (IMR90) are reprogrammed after stable expression of either NBR1-specific shRNA (shNBR1) or non-targeting shRNA (shNT). Emerging iPSC colonies are scored based on Tra-1-60 expression[37]. (a, b) Cells depleted of NBR1 to increase MB^{d} levels show an increase in iPSC colony formation (a, dH1f: 3.1±0.5-fold, n=15, p=0.00035; IMR90: 3.4±0.8-fold, n=3, p=0.02; data are mean ± s.e.m.) but insignificant changes in autophagic activity (c) over shNT control. (b) Representative plates with Tra-1-60-immunostained iPSC colonies. Immunoblot (c, top) and densitometry (c, bottom; percent of autophagic flux) show representative result (n=3); α-tubulin, loading control. (**d**) MCF-7 side-population (SP) cells have a significantly higher percentage of MB^{d}+ cells over the non-SP population (MP; p=0.0015, n=3; data are mean ± s.d.). (**e**, **f**) MB^{d} enrichment in cancer cells leads to increased anchorage-independent growth. MKLP1-GFP-expressing

HeLa cells are separated into "MB^d high" and "MB^d low" subpopulations. An increase in the "MB^d high" over "MB^d low" ratio is associated with an increase in soft-agar colony formation (e). No significant difference was observed when the enrichment of MB^d high subpopulation was less than 3-fold. More soft-agar colonies are formed when MB^ds are enriched by NBR1-depletion (shNBR1) in HeLa (f, left; p=0.0012, n=3) and mouse 134-4 cells (f, right; p=0.0086, n=3); control, shNT. Data are mean ± s.d., and the colony number (e, f) is the sum of INT-violet-stained colonies from 10 random fields. (**g**) Model for MB^d fate in cells. The newly-formed MB^d is preferentially inherited by the daughter cell with the older centrosome (top panel). The inherited MB^d (black ring) is recognized by binding of the NBR1 autophagic receptor (grey circle) with the MB protein Cep55 (magenta). The MB^d is then encapsulated by the autophagosome (yellow circle), and degraded after fusion of autophagosome and lysosome (red circle) in differentiated cells. This pathway prevents MB^d-accumulation. In contrast, stem cells efficiently accumulate MB^ds through successive divisions and evasion of NBR1-mediated autophagy. Additionally, differentiated and stem cells possess overall high and low autophagic activity, respectively.